



This is a repository copy of *Local buckling in cold-formed steel moment-resisting bolted connections : behavior, capacity and design*.

White Rose Research Online URL for this paper:
<http://eprints.whiterose.ac.uk/158874/>

Version: Accepted Version

Article:

Mojtabaei, S.M., Becque, J. and Hajirasouliha, I. orcid.org/0000-0003-2597-8200 (2020) Local buckling in cold-formed steel moment-resisting bolted connections : behavior, capacity and design. *Journal of Structural Engineering*, 146 (9). ISSN 0733-9445

[https://doi.org/10.1061/\(ASCE\)ST.1943-541X.0002730](https://doi.org/10.1061/(ASCE)ST.1943-541X.0002730)

This material may be downloaded for personal use only. Any other use requires prior permission of the American Society of Civil Engineers. This material may be found at <https://ascelibrary.org/doi/10.1061/%28ASCE%29ST.1943-541X.0002730>.

Reuse

Items deposited in White Rose Research Online are protected by copyright, with all rights reserved unless indicated otherwise. They may be downloaded and/or printed for private study, or other acts as permitted by national copyright laws. The publisher or other rights holders may allow further reproduction and re-use of the full text version. This is indicated by the licence information on the White Rose Research Online record for the item.

Takedown

If you consider content in White Rose Research Online to be in breach of UK law, please notify us by emailing eprints@whiterose.ac.uk including the URL of the record and the reason for the withdrawal request.



eprints@whiterose.ac.uk
<https://eprints.whiterose.ac.uk/>

Local buckling in cold-formed steel moment resisting bolted connections: behaviour, capacity and design

Seyed Mohammad Mojtabaei¹, Jurgen Becque², Iman Hajirasouliha³

¹Ph.D. Student, Dept. of Civil and Structural Engineering, Univ. of Sheffield, Sheffield S1 3JD, UK (corresponding author). ORCID: <https://orcid.org/0000-0002-4876-4857>. Email: smmojtabaei1@sheffield.ac.uk

²Lecturer, Dept. of Civil and Structural Engineering, Univ. of Sheffield, Sheffield S1 3JD, UK. Email: j.becque@sheffield.ac.uk

³Senior Lecturer, Dept. of Civil and Structural Engineering, Univ. of Sheffield, Sheffield S1 3JD, UK. ORCID: <https://orcid.org/0000-0003-2597-8200>. Email: i.hajirasouliha@sheffield.ac.uk

Abstract

The research presented in this paper aimed to investigate local buckling failure occurring adjacent to moment resisting bolted connections in cold-formed steel back-to-back channel beams connected to a gusset plate through their webs. This failure is a result of a complex stress state originating from the transfer of both shear and bending moment through the web, combined with important shear lag effects. Experimentally validated finite element models were used, accounting for material nonlinearity, geometric imperfections and non-linear bolt bearing behaviour. The effects of the cross-sectional shape and thickness of the beam, the bolt group configuration and the bolt group length were investigated. It was discovered that the detrimental effect of local buckling exponentially decreases when a longer bolt group length is used, when the load is introduced at the connection with a smaller eccentricity relative to the centroid, and when the thickness of the beam is increased. The results of the investigation were employed to develop a practical design equation with a wide range of applicability. Finally, a reliability analysis was performed within the framework of both the Eurocode and the AISI standards.

Key words: cold-formed steel; portal frames; bolted connection; local buckling; design equation; reliability analysis

1 Introduction

CFS portal frames are fundamentally different from hot-rolled frames in the way the connections are conceived. They are typically bolted connections and consist of steel gusset plates, usually featuring folded edge stiffeners (and in those cases sometimes referred to as 'brackets'), to which the webs of the connecting members are bolted. Fig. 1 shows typical arrangements for an eave and an apex connection between back-to-back channel members. These types of connections are economical and easy to assemble. However, the fact that a connection is made through the webs of the connecting members only, leaving the flanges unconnected, has obvious repercussions for the behaviour of the connection, both in terms of stiffness (they typically act as semi-rigid connections with a stiffness governed by the bolt hole elongation characteristics) and strength. With respect to the latter, in a connection with properly sized bolts and gusset plates failure typically takes place in the connecting member, adjacent to the connection, as a result of cross-sectional instability [2-5]. This instability is promoted by the introduction of both moment and shear through the web only, whereby the local stress concentrations at the bolt locations can potentially further reduce the capacity below the calculated cross-sectional values. Unfortunately, current design standards do not account for this type of failure, which was first observed by Kirk [6] in tests on CFS back-to-back lipped channel portal frame connections as early as 1986. It is also consistent with observations reported by Chung and Lau [7] on CFS moment resisting bolted connections.

Lim [8] conducted a comprehensive study on CFS moment resisting bolted connections, which also considered various failure modes of the bracket: overall lateral-torsional buckling and local buckling modes of the bracket components. A large part of the study, however, was devoted specifically to local web buckling of the connecting members. With this purpose an experimental program was carried out consisting of four apex connections tested in a four-point bending configuration, described in detail in [9]. The tests revealed a profound influence of the bolt group length l_b (i.e. the distance between the centre lines of the outer bolt rows, as indicated in Fig. 2) on the capacity of the connections. The authors explained this by pointing out the reduced magnitude of the bolt forces in the longer connection. While this is of course true, the change in inclination of the bolt force in the shorter connection should also be noted. While the bolt forces in the first row of the longer connection are near vertical, a comparatively much larger horizontal component is introduced into the portion of the web adjacent to the connection in the shorter bolt group. This horizontal force adds to the compression already present as a result of bending and

increases the risk of local buckling in the web of the connected member just outside the bolt group.

Lim et al. [10] dedicated a further study to the development of a design methodology for this type of connections based on the Direct Strength Method (DSM). The authors borrowed ideas from previous work by Baigent and Hancock [11], who conducted experiments on frames composed of single CFS channels with rigid connections. Baigent and Hancock drew attention to the effect of the bi-moment in the channels, which reduced their capacity below the major axis bending capacity. Lim et al. [10] claimed that this bi-moment is also important in back-to-back channel connections where a moment is introduced eccentrically in the web of each individual channel. Consequently, they proposed to calculate the connection capacity using the DSM local buckling equations, but with an elastic buckling stress obtained from a finite strip analysis in which the stress distribution resulting from a combined bending moment and bi-moment is applied. It was concluded that this results in conservative predictions for bolt groups with reasonable lengths ($l_b/h > 1$, where h is the section depth), with the margin of safety increasing with the bolt group length l_b .

Dubina et al. [5] tested a total of nine eaves joints and nine apex joints between back-to-back lipped channel members, including a limited number of specimens with additional bolts in the flanges. The specimens were tested under either monotonic or cyclic loads. The authors also investigated the applicability of the component method to predict the stiffness and strength of these connections. In addition, two tests on full-scale portal frames under monotonically increasing lateral loading (in one case combined with vertical pre-loading) were carried out.

In other noteworthy research Chung and Lau [7] tested six CFS bolted beam-to-column connections under a linearly varying moment in the beam. Four of the connections failed by lateral-torsional buckling of the gusset plate, while the others failed by local buckling of the web. Wong and Chung [12] carried out 20 tests on both column base connections and beam-to-column connections. They observed four different failure modes, namely bearing failure of the bolts, lateral-torsional buckling of the gusset plate, flexural failure of the gusset plate and flexural failure of the beam. The latter mode corresponded to the local buckling failure of the web previously discussed. Öztürk and Pul [13] carried out four-point bending tests on apex connection between back-to-back sigma channel rafters. Different connection configurations and stiffening arrangements of the bracket were considered. The study focused on local buckling of the bracket and local buckling of the beam web as failure modes.

Bučmys et al. [14] developed a component model for CFS joints consisting of three rotational springs, representing the stiffnesses of the bolt group in the beam, the gusset plate and the bolt group in the column. A comparison with experimental results confirmed the accuracy of the proposed model. Sabbagh et al. [15] conducted cyclic tests to evaluate the hysteretic behaviour of CFS beam-to-column bolted connections. The test specimens had an unusual cross-sectional shape with curved flanges. Unstiffened webs, as well as web reinforced with welded-in stiffeners were considered.

Rinchen and Rasmussen [16] experimentally and numerically investigated the flexural behaviour of eaves, apex and base connections of portal frames composed of single CFS channels. The apex connections failed by inelastic buckling near the junction of the compression flange and the web, while the eaves connections failed by fracture of the screws or bearing of the bolts. It was also reported that the base connections exhibited large rotational deformations as a result of concentrated inelasticity in the connector bracket.

The same investigators also conducted full-scale tests on long-span portal frames with single CFS channel members, subjected to gravity loading or combined gravity and lateral loading, to investigate their structural performance and strength [17]. It was observed that flexural-torsional buckling of the columns was the dominant failure mode. The experimental results also revealed that the ultimate failure deformations were determined by the type of fasteners used to connect the channel lips to the brackets in the apex and eaves connections. The ultimate capacities of the tested frames were lower than those determined according to the Direct Strength Method, which was attributed to the presence of a bimoment induced at the connections in the test frames. In a follow-up, study a comprehensive numerical investigation using detailed FE models was conducted to assess the nonlinear load-displacement response of the portal frames [18]. The investigators further proposed design approaches for portal frames consisting of single CFS channels based on the Direct Strength Method and the Direct Design Method, which considered the influence of the bimoment on the capacity of the CFS members [19].

Blum and Rasmussen [20] carried out experiments on portal frame systems consisting of three frames connected in parallel with purlins to investigate the effect of various design parameters, in particular the configuration of the knee connection, the presence of sleeve stiffeners and the type of loading, on the capacity and the failure modes of the frames. The frames were composed of back-to-back lipped channels. In a related study the same investigators used an experimentally validated FE model of a haunched portal frame to

conduct parametric studies, in which the effects of the connection stiffness and configuration on the frame capacity and behaviour were studied [21]. In addition, an experimental program was conducted to quantify the column-to-base connection stiffness for different thicknesses and configurations of the bracket, and the in-plane stiffness of the apex connection for different rafter channel thicknesses and depths.

Zhang et al. [22] carried out experimental investigations of the structural performance of CFS pitched portal frames subject to local and distortional buckling under different combinations of horizontal and vertical loads. The study revealed that the current AS/NZS4600 and AISI-S100 design standards may overestimate the capacity of locally and distortional buckled portal frames. In a follow-up study, Zhang et al. [23] compared the results of a portal frame test with those obtained from FE models using two different types of elements, namely shell and modified beam elements. Good agreement was obtained in both cases.

Tshuma and Dunda [24] studied 2-bay CFS portal frames comprised of single channels and developed two new configurations for the connection between the rafters and the internal column. The configurations were experimentally investigated and local buckling originating in the compressed portion of the web and later spreading to the flanges was found to be the governing failure mode in both cases. Pouladi et al. [25] numerically studied eaves connections in single channel portal frames containing both screws and bolts. It was concluded that the screws failed in shear before the bolts had fully slipped.

Despite the significant amount of research conducted on CFS portal frame connections to date, a number of additional issues need to be addressed in order to support and facilitate practical design:

1. The design equations previously proposed by Lim and Nethercot [9] for CFS moment resisting bolted connections are only valid within a certain range of design parameters. Most importantly, they were developed for back-to-back lipped channels with specific dimensions. There is an obvious need for a more universally applicable design methodology given the wide range of beam sections available in practice.
2. The previously developed design equations [9] considered the influence of the relative bolt group length (l_b/h), the web slenderness (h/t) (where t is the section thickness) and the geometric arrangement of the bolts (in 2x2, 3x3 and 4x4 patterns). However, as will be shown in this paper, the connection capacity also exhibits a major dependence

on the eccentricity parameter X , which is defined as the distance between the web and the centroid of the cross-section, necessitating an update of the design equations.

3. Before applying the proposed equations in practical design a reliability study needs to be carried out in order to demonstrate that the design equations possess the required margin of safety.

This paper aims to address all of the above issues. The scope of the current paper will however be limited to local buckling failure in the web and excludes other failure modes such as bolt failure and failure of the gusset plate.

2 Finite element model and validation

Finite element (FE) modelling has previously been used to predict the behaviour of CFS bolted connections [9, 13, 26-31] and good agreement between the test results and the FE predictions has generally been reported. In this study the experimental work by Lim and Nethercot [9] was used to validate an FE model which was developed in the software package ABAQUS [22] with the purpose of further investigating these types of connections. Lim and Nethercot conducted an experimental study on apex joints using the four-point bending configuration illustrated in Fig. 2, while varying the length l_b of the bolt group between tests. More specifically, the l_b/h ratio ranged from 0.94 to 1.83 in joints A to D, as detailed in Fig. 2. The connected members consisted of back-to-back lipped channels with the dimensions shown in Fig. 2.

2.1 Geometry and boundary conditions

The geometry and boundary conditions of the experimental set-up were replicated in the FE model, as shown in Fig. 3. To simulate pin-ended boundary conditions at the specimen ends, the nodes belonging to each end section of the back-to-back channels were first coupled to the centroid of the whole cross-section, where a reference point was defined. Simply supported boundary conditions were then applied to the reference points at both ends, as clarified in Fig. 3. The lateral displacements of the webs were prevented at those locations where bracing was put in place during the test, as also shown in Figs. 2 and 3. Finally, point loads were applied in a displacement controlled manner to reference points which were coupled to all the nodes of the cross-section at the load application points.

2.2 Element type and material properties

Shell elements are the logical choice for thin-walled structures, where the thickness is typically considerably smaller than the other dimensions. The general-purpose S4R element, which is a 4-noded quadrilateral flat shell element with reduced integration, was selected

from the ABAQUS library. The default setting of five integration points over the thickness was used. This particular element was previously shown by other researchers to yield accurate predictions when modelling CFS connections subject to bending [27, 32]. To select an appropriate mesh size, a mesh sensitivity analysis was carried out using the model for connection D (see Figure 2). The results are shown in Table 1 and the conclusion can be drawn that refining the mesh beyond a $20 \times 20 \text{ mm}^2$ size had a negligible effect on the predicted connection capacity. Consequently, a mesh size of $20 \times 20 \text{ mm}^2$ was selected.

The material behaviour was modeled using a bi-linear stress-strain diagram with an initial elastic modulus $E=210 \text{ GPa}$, followed by a linear hardening range with a slope of $E/100$. This model was previously proposed by Haidarali and Nethercot [33]. The yield stress and the ultimate strength, as measured from coupon tests reported in [9], were $f_y=358 \text{ MPa}$ and $f_u=425$, respectively, for the channels, and $f_y=341 \text{ MPa}$ and $f_u=511 \text{ MPa}$ for the gusset plate.

2.3 Modelling of the bolts

It has previously been shown that the bearing characteristics of the bolts (i.e. the initial bearing stiffness and the inelastic bolt hole elongation stiffness) have a considerable influence on the rotational capacity of a bolted CFS connection, but only have a minor effect on its ultimate capacity [15, 34]. One option to model the bolt behaviour, used by several researchers in the past [13, 35, 36], is to explicitly model the geometry of the bolts, nuts and washers using solid elements and surface-to-surface interactions. However, this typically leads to a complex model which is computationally expensive, especially in connections with a large number of bolts. Lim and Nethercot [3, 9] therefore employed a simplified bolt model consisting of two perpendicular linear elastic springs. They reported good agreement between the FE predicted flexural capacity of the connections and the experimental values. It should be noted, however, that all connections in [9] failed by cross-sectional instability in the channel beams in the zone adjacent to the connection and not by failure of the actual connection. Similarly, the main focus of the study presented in this paper was to determine the capacity of the connected CFS member, as limited by cross-sectional instability, and it could therefore be argued that the modelling of the bolt behaviour was of secondary importance. However, the ability to model the actual moment-rotation behaviour of the connection zone and verify it against the experimentally recorded behaviour reported in [9] was believed to constitute a valuable addition to the study and one thought to be relevant in light of planned further studies related to rotational capacity and associated energy

dissipation under monotonic and cyclic loading. The bolts were therefore modelled using ‘discrete fastener’ elements from the ABAQUS library [37] which permitted the input of the actual inelastic bolt hole elongation behaviour. The bearing behaviour of the bolts used in the tests was experimentally investigated by Lim and Nethercot [26] through double lap shear tests. The resulting load-elongation graph, shown in Fig. 4, was used in the validation process. However, in further parametric studies, which included plate thicknesses different from those reported in [16], the equations proposed by Fisher [38] were adopted instead:

$$R_B = R_{ult} \left[1 - e^{-\mu(\delta_{br}/25.4)} \right]^\lambda \quad (1)$$

$$R_{ult} = 2.1 \cdot d \cdot t \cdot F_u \quad (2)$$

In the above equations δ_{br} is the bearing deformation (in mm), R_{ult} is the ultimate bearing strength, t is the web thickness, d is the bolt diameter and R_B is the bearing force in the bolt. F_u is the tensile strength of the web material, while $\mu = 5$ and $\lambda = 0.55$ are regression coefficients presented by Uang et al. [39]. The bolt diameter was reported to be 16 mm in [9] and this value was maintained throughout the parametric studies. It should be noted that Eq. (1) ignores bolt slip.

The ‘discrete fastener’ elements in ABAQUS make use of attachment lines to create connectors between selected faces of surfaces, as shown schematically in Fig. 5. The three surfaces in this figure represent the two webs of the channels and the gusset plate in between. A ‘radius of influence’ is assigned to each connector, whereby the displacements and rotations of the surface nodes within this radius are coupled to the displacements and rotations of the fastening point. This radius was taken as 8 mm. However, a sensitivity study varying the radius of influence between 5 mm and 30 mm indicated that this variable had negligible influence, with the corresponding capacity predictions varying by only 2%.

2.4 Imperfections

Lateral-torsional buckling of the test specimens in [9] was prevented by the presence of a lateral bracing system and all specimens failed by cross-sectional instability in the zone adjacent to the connection. Therefore, either a local or a distortional imperfection was incorporated into the model, depending on which mode had the lower critical buckling stress. This was achieved by carrying out an elastic buckling analysis of the apex connection in ABAQUS and using the scaled first eigenmode as the shape of the initial imperfection. The amplitude of the imperfection was determined based on the work by Schafer and Peköz [40],

whereby the 50% value of the cumulative distribution function of the imperfection magnitudes was adopted. This represents the ‘most likely’ imperfection and amounts to a magnitude of $0.34t$ and $0.94t$ for the local and distortional imperfections, respectively. It should be noted, however, that the aforementioned work [30] was based on data pertaining to CFS sections with thicknesses below 3 mm. It therefore directly applies to the modelling of the experimental programme carried out by Lim and Nethercot [9] in the validation study. However, further parametric studies were carried out for thicknesses (t) which in some cases exceeded 3 mm (see Section 3). In those models the imperfection magnitude was determined using the equation proposed by Walker [41]:

$$\omega_d = 0.3t \sqrt{\frac{\sigma_{0.2\%}}{\sigma_{cr}}} = 0.3t\lambda_s \quad (3)$$

where $\sigma_{0.2\%}$ and σ_{cr} are the 0.2% proof stress of the material and the elastic local buckling stress of the cross-section, respectively, and λ_s is the cross-sectional slenderness, calculated as:

$$\lambda_s = \sqrt{M_y / M_{cr}} \quad (4)$$

In Eq. (4) $M_y = Z_f f_y$ is the yield moment of the cross-section and $M_{cr} = Z_f \sigma_{cr}$ is the elastic local buckling moment. Z_f is the elastic section modulus about the axis of bending. σ_{cr} can be computed using software such as CUFSM [42], which is based on the finite strip method.

While this approach was motivated by the lack of actual imperfection measurements in the experimental programme, a sensitivity study previously carried out by Lim and Nethercot [9] has demonstrated that this particular failure mode can be considered to be rather insensitive to the imperfection magnitude, thus largely justifying the adopted methodology.

2.5 Validation of FE model

The four connections A to D, representing apex connections with different bolt group lengths, were analyzed using a “Static General” analysis. As an example, Fig. 6 shows the moment in the constant moment span versus the vertical apex displacement of connections A and D obtained from the experiments, as well as the corresponding curves predicted by the FE model. It should be mentioned that the initial gradual increase in the gradient of the experimental moment-deflection curve of connection A was reported to be due to imperfect alignment of the bolt holes and slack in the loading rods [9]. Hence, this experimental curve

was modified by first determining the connection stiffness at a bending moment of 40 kNm, extending the curve down from this point to the horizontal axis with the same stiffness and then shifting the curve to the origin. It is seen that the FE results agree well with the experimental observations over the whole loading range up to the peak load. Concurrently, Table 2 demonstrates that the proposed FE model predicts the moment capacity (M_{max}^{FE}) of all apex connections very well compared to the experimental results (M_{max}^{exp}), with an average error of 2% and a standard deviation of 0.018. The failure mode of local buckling adjacent to the connection observed in the experiments was also correctly replicated by the FE models.

2.6 Simplification of the apex connection model

In order to simplify the FE model for further investigations the apex connection in four-point bending was alternatively modelled as a cantilever beam with a bolted gusset plate connection subjected to pure bending moment. Fig. 7 illustrates the FE model and indicates the loading and boundary conditions. The gusset plate was fixed (clamped) at its end and connected to the back-to-back channels by means of fastener elements. At the loaded end of the beam, the rotational degrees of freedom about the x- and y-axis of all points in the cross-section were coupled to those of the centroid, while an increasing major axis rotation was applied. The beam was supported in the out-of-plane direction along the web edges to prevent lateral-torsional buckling. A sensitivity study was carried out using connections with two different bolt group lengths ($l_b/h = 0.5$ and $l_b/h = 3$, which could be considered to constitute the practical extremities of the l_b/h spectrum) in order to determine an appropriate value of the cantilever length l_e (see Fig. 8), expressed as a multiple of the cross-sectional depth ($l_e = \omega h$). This study is necessary since the boundary conditions at the loaded end prevent warping of the cross-section and thus, for an insufficient length, restrain the shear lag effect which occurs at the bolted connection (as discussed in Section 3.2), resulting in an increased capacity. The results presented in Fig. 8 indicate that the predicted moment capacities converged past $\omega = 6$ for both bolt group lengths. Hence, an effective length (l_e) equal to $6h$ was used in further parametric studies.

The failure mode of connections A to D predicted by these simplified FE models is local buckling of the web immediately adjacent to the first bolt line, as shown in Fig. 9 for connections A and D. This is consistent with the experimental observations, as well as with the more detailed FE models. The predicted moment capacities ($M_{max}^{S,FE}$) of connections A-D

also agree very well with the experimental results, as shown in Table 2, with a negligible average error and a standard deviation of 2.7 %.

3 Parametric studies

The simplified FE model described in the previous section was further used to conduct parametric studies. Table 3 lists the selected variables. Three distinct bolt group arrangements were considered, containing bolts in 2x2, 3x3 and 4x4 arrays. Within each configuration the ratio of the bolt group length to the section depth l_b/h was varied from 0.5 to 3.0 in intervals of 0.25. Five different cross-sectional geometries were considered. They consisted of conventional back-to-back lipped channels with progressively wider flanges and a shallower web (Table 4). The underlying aim was to vary the parameter X , which is the distance from the centroid of the channel to the centreline of the web. In addition, four different section thicknesses $t=1, 2, 4, \text{ and } 6$ mm were considered for each channel geometry in order to vary the cross-sectional slenderness (λ_s), which is defined by Eq. (4). The values of λ_s corresponding to the cross-sections comprised in the parametric studies are also listed in Table 4. The yield stress f_y , the elastic modulus E and the Poisson's ratio of the material ν were taken as 313 MPa, 210 GPa and 0.3, respectively. The thickness of the gusset plate was kept constant at 12 mm, which was thick enough to avoid any premature failure in the gusset plate. A total of 660 FE models were needed to systematically investigate the effects of the aforementioned variables on the capacity of the connection and to achieve this the ABAQUS Scripting Interface [37] based on the object-oriented programming language Python was used.

3.1 Results

The moment capacity of a CFS beam at the gusset plate connection (M_c) can be expressed as:

$$M_c = R M_u \quad (5)$$

where M_u is the cross-sectional moment capacity of the beam and R is a reduction factor accounting for the fact that local web buckling adjacent to the connection may prevent the full cross-sectional bending strength M_u from being reached. The reduction factor R is assumed to be a function of the previously selected variables, including the bolt group length l_b/h , the bolt group arrangement and the channel geometry and thickness.

For the purpose of evaluating Eq. (5) the cross-sectional moment capacity M_u of a given CFS beam was obtained from an FE analysis of a beam segment subjected to pure bending moment. The FE model shown in Fig. 7 was used for this purpose, except that the gusset plate and the connector elements were removed from the model and equal and opposite rotations were applied to both ends of the beam. The beam, however, remained laterally restrained along the web-flange junctions. The length of the beam segment was taken as three times the distortional buckle half-wave length, calculated using the CUFSM [42] software, as suggested by Shifferaw and Schafer [43]. The values of M_u obtained for the different cross-sections and thicknesses under consideration are listed in Table 4.

Figures 10-12 present the results of the parametric studies in terms of the R values. The graphs show that, for a given cross-section and bolt group arrangement, the R values exponentially approach 1 for increasing l_b/h values. This is confirmed by plotting $\ln(1 - R)$ versus l_b/h , as illustrated in Fig. 13 for the data related to a 3x3 bolt group. This finding dislodges earlier suggestions by Lim and Nethercot [9] that the trend is logarithmic rather than exponential. Moreover, the group of curves in Fig. 13 display a fan shape and appear to have the tendency to pass through a single point on the vertical axis, suggesting an equation of the form:

$$1 - R = C_1 e^{[S(\frac{X}{t})](\frac{l_b}{h})} \quad (6)$$

where C_1 is a constant and S is a currently unknown function. Further analysis of the gradients S of the lines in Fig. 13 as a function of X/t revealed that the data trends can be accurately captured using an equation of the following form:

$$R = 1 - C_1 e^{-C_2 (\frac{l_b}{h})(\frac{t}{X})} \quad (7)$$

where C_1 and C_2 are constants. The fact that R is dependent on the product of l_b/h and t/X allows the alternative interpretation that the moment capacity is instead governed by the parameters (h/t) , which constitutes the slenderness of the web (and thus determines the susceptibility to local buckling) and (X/l_b) , which has also been used in the AISI [44] guidelines as a parameter determining the severity of the effect of shear lag in a tensile connection.

MATLAB [45] was used to determine the constants C_1 and C_2 in Eq. (7) from an optimization problem. The procedure minimized an error measure, which was taken as the

standard deviation of the ratio (R_{pred}/R_{FE}). R_{pred} is the R value predicted by Eq. (7), while R_{FE} is the corresponding R value resulting from the numerical simulations. The ensuing equations are listed in Table 5, together with their statistical indicators.

Figs. 10 to 12 graphically compare the reduction factors R predicted by Eqs. (8-10) to the FE analysis results for the 2x2, 3x3, and 4x4 bolt configurations, respectively. Good agreement between the predictions and the numerical data is visually observed, confirming the favourable statistics in Table 5.

It is noted that the proposed equations for the 3x3 and 4x4 bolt group configurations lead to only minutely different predictions of R , so that Eq. (10) can be adopted for both 3x3 and 4x4 bolt groups. Eq. (8) for the 2x2 bolt group leads to slightly lower values of R . However, the difference is relatively small, so that an attempt to unify Eqs. (8-10) into a single universally valid design equation appears justified. This was achieved by applying the same optimization procedure to the full set of 660 data points, resulting in the following equation:

$$R = 1 - 0.42e^{(-13.8(\frac{t}{X})(\frac{l_b}{h}))} \quad (11)$$

Evaluated over all data Eq. (11) displayed an average ratio of (R_{pred}/R_{FE}) of 0.97 with a standard deviation of 0.02.

3.2 Discussion of the results

In order to further investigate the physical phenomena which underlie the dependence of the moment capacity on the bolt group length l_b/h , thickness t and eccentricity X , Table 6 shows the various stress profiles in the beam extracted from the FE models for a range of these parameters. The stresses were evaluated in the initial elastic range, before local buckling or plasticity took hold. However, a small imperfection was included in the models, as previously explained in Section 2.4. The profiles represent the stress state in the beam section located at the end of the gusset plate, a distance of $1.5d$ removed from the first bolt row, which is representative of the location of failure. Only the two extremes of the bolt group length spectrum considered in this study are represented in Table 6: a first case which corresponds to a short bolt group with $l_b/h= 0.5$ and a second case which represents a much longer bolt group with $l_b/h= 3$. All results pertain to a 3x3 bolt group. However, similar observations were made for the other bolt group configurations.

It is seen that the stress profile differs significantly across these examples, mainly depending on the bolt group length, but with additional influence of the channel thickness and eccentricity. In particular, it is clear that the stress profile in the channels with the longer bolt group bears a much closer resemblance to the expected linear stress gradient over the section height predicted by classical beam theory. On the other hand, the flanges in the channels with the shorter bolt group display a stress gradient with decreasing contribution towards the lip, while the stress profile in the web also deviates more from the expected linear trend. The difference in stress behaviour between short and long bolt groups becomes more pronounced as the eccentricity of the centroid relative to the web increases (i.e. when progressing from channel Ch1 to channel Ch5), while the thickness also has an influence. The thickest channels ($t= 6$ mm) show stress profiles for $l_b/h= 3$ which agree most with the predictions of beam theory, while the thinnest channel ($t= 1$ mm) with $l_b/h= 0.5$ and the largest eccentricity (Ch5) has the strongest varying stress profile across the flanges, with stress reversal even taking place at the flange-lip junction. A possible explanation for this phenomenon was put forward in [10], where the researchers argued that it is caused by the presence of a bi-moment in the connection. Indeed, the bending moment is introduced in the plane of the channel web by the bolts in the connection. If this moment is resolved, for the sake of reasoning, into a couple of forces acting at the level of the flanges, then each force will cause in-plane bending of the flange, but in an opposite direction in each flange, thus producing a stress profile similar to the one observed for $l_b/h= 0.5$. Lim et al. [10] proposed to calculate this bi-moment as the product of the moment and the distance from the web to the shear centre. While the argument that a bi-moment is introduced cannot completely be discarded, the counterargument can be put forward that this bi-moment is largely counteracted by axial forces in the bolts, which force the web of the channel to remain in contact with the gusset plate and thus eliminate any twist in the channel necessarily associated with a bi-moment. It therefore does not seem sensible to design the critical cross-section of the beam just outside the connection for the full bi-moment, specified as above, in combination with the applied bending moment. To strengthen this argument one can point out that a parallelism exists in the design of an eccentric tensile connection, where a tensile member is never designed for a moment equal to the product of the tensile force with the eccentricity, in addition to the actual tensile force. Rather it is assumed that the bolted connection largely counteracts any tendency of end rotation in the member. In the practical design of these connections a reduction factor is typically applied to the tensile capacity of the member to account for the eccentricity with which the force is

introduced into the member at the connection. The accepted explanation is that this reduction factor accounts for the shear lag effect, i.e. the fact that a certain distance along the member is required for the forces introduced into the connected plate element to spread out into the other parts through longitudinal shear stresses.

In the authors' opinion, the mismatch between the stress distribution predicted by classical beam theory and those pictured in Table 6 can equally be interpreted as the result of a shear lag effect. This effect exists because the bending moment is introduced by the connection into the plane of the web and subsequently has to spread out into the flanges, with the flange tips initially lagging behind the web in longitudinal strains. An approach similar to the one used for eccentric tensile connections, with a reduction factor applied to the cross-sectional bending capacity to account for the shear lag effect, was therefore preferred.

It is clear that a larger shear lag effect will generally develop for larger values of the eccentricity X between the web and the centroid of the cross-section and this is in agreement with the observations from Table 6. On the other hand, the length of the bolt group affects the phenomenon by influencing the direction of the bolt shear forces, which are required to remain perpendicular to the line connecting each bolt to the centre of the bolt group (Fig. 14). Consequently, a longer bolt group will lead to the moment being introduced into the web mainly by vertical forces (which are also smaller in magnitude). However, since the web naturally carries the bulk of the shear force, these vertically introduced forces do not require any major redistribution of stresses. Horizontal components of the bolt forces, however, as significantly present in shorter bolt groups, will need to find their way into the flanges through shear lag. At the same time, the compressive part of the web adjacent to these connections needs to carry a disproportionate amount of stress relative to the predictions of beam theory, resulting in an increased susceptibility to local web buckling.

The above explanations comprehensively account for the observed differences between the various cases pictured in Table 6, something which cannot be achieved in an entirely satisfactory way by the theory in [10]. Indeed, an identical bi-moment would presumably be present in all cases associated with a particular cross-sectional geometry (Ch1 to Ch5), while Table 6 indicates that very different stress profiles originate within each group.

4 Reliability analysis

In order to ensure that the proposed design equations provide the required margin of safety, a reliability analysis was performed within the framework of both the Eurocode (CEN 2002) [46] and the AISI specifications [47]. To ensure a sufficiently small probability of failure, the reliability index β must exceed a specific target value. For new structures with a design working life of 50 years and a consequence class rated as CC2 (moderate consequences of failure), the Eurocode prescribes a reliability index of 3.8 [46], while the AISI specifications prescribe $\beta=2.5$ for CFS flexural members and $\beta=3.5$ for connections [47]. Since the failure mode under consideration was local buckling of the beam outside the actual bolted connection, $\beta=2.5$ was considered when using the AISI framework. In the Eurocode for structural steel, resistances are divided by a partial safety factor γ , while in the AISI specifications they are multiplied by a resistance factor ϕ . The required nominal resistances are determined from load combinations involving the nominal values of the dead load D_n and the live load L_n , as follows:

$$\frac{R_n}{\gamma} = \gamma_D D_n + \gamma_L L_n \text{ (Eurocode)} \quad \text{or} \quad \phi R_n = \gamma_D D_n + \gamma_L L_n \text{ (AISI)} \quad (12)$$

In the Eurocode $\gamma_D=1.35$, and $\gamma_L=1.5$, while in the AISI code $\gamma_D=1.2$, and $\gamma_L=1.6$. Both standards consider the design resistance r_d to be equal to the load ($\gamma_D D_n + \gamma_L L_n$) in their reliability analyses, which implies a full use of the resistance, without reserve capacity.

Based on Annex D of Eurocode 0 [46] the design resistance r_d can be determined as follows:

$$r_d = b_1 \cdot b_2 \cdot r_m \cdot e^{-[k_{d,\infty} \alpha_R Q_n + k_{d,n1} \alpha_{\delta 1} Q_{\delta 1} + k_{d,n2} \alpha_{\delta 2} Q_{\delta 2} + 0.5 Q^2]} \quad (13)$$

The factors b_1 and b_2 replace the original factor b specified in Annex D, to account for the fact that the model uncertainty in the applied methodology has two sources: b_1 accounts for the deviation of the predicted resistance from the FE model, while b_2 accounts for the FE model uncertainty relative to the experiment. r_m is the resistance determined using the mean values of all relevant variables. The assumed probabilistic distributions of the basic variables are listed in Table 7, based on recommendations in the literature [48, 49]. Further to Eq. (13), $k_{d,\infty} = \alpha_R \beta = 3.04$, where α_R is a sensitivity factor which Eurocode 0 recommends to take equal to 0.8. The factor $k_{d,n1}$ depends on the number of FE results the

design equation is validated against, which is 660 in this case, and thus, according to Table D2 of Eurocode 0: $k_{d,n1} = 3.04$. The factor $k_{d,n2}$, on the other hand, depends on the number of experiments used to validate the FE model. Standing at four, this number is relatively low, which, again according to Table D2 of EC 0, necessitates the rather conservative assumption that $k_{d,n2} = 11.4$.

The correction factors b_1 and b_2 are defined as the slope of the least squares regression line in the M_{FE} versus M_c and the M_{Test} versus M_{FE} diagram, respectively:

$$b_1 = \frac{\sum (M_c \cdot M_{FE})}{\sum (M_c)^2} \quad (14)$$

and:

$$b_2 = \frac{\sum (M_{Test} \cdot M_{FE})}{\sum (M_{FE})^2} \quad (15)$$

M_{Test} is the moment capacity measured in the experiment, M_{FE} is the moment capacity obtained from the FE models and M_c is the moment capacity predicted by the design equation. Using the available data b_1 and b_2 were found to be equal to 1.28 and 0.99, respectively. Eurocode 0 also requires the calculation of the error terms δ_1 and δ_2 , corresponding to b_1 and b_2 , which are determined by:

$$\delta_1 = \frac{M_{FE}}{b_1 M_c} \quad (16)$$

$$\delta_2 = \frac{M_{Test}}{b_2 M_{FE}} \quad (17)$$

The variables Q_{rt} , Q_{δ_1} , Q_{δ_2} and Q featured in Eq. (13) represent the standard deviation of the resistance calculated using the proposed design equation, the standard deviation of the error terms δ_1 and δ_2 , and the overall standard deviation of the resistance, respectively. These standard deviations were calculated based on the assumption of lognormal distributions as follows:

$$Q_{rt} = \sqrt{\ln(V_{rt}^2 + 1)} \quad (18)$$

$$Q_{\delta_1} = \sqrt{\ln(V_{\delta_1}^2 + 1)} \quad (19)$$

$$Q_{\delta_2} = \sqrt{\ln(V_{\delta_2}^2 + 1)} \quad (20)$$

$$V_r^2 = V_{\delta_1}^2 + V_{\delta_2}^2 + V_{rt}^2 \quad (21)$$

$$Q = \sqrt{\ln(V_r^2 + 1)} \quad (22)$$

In the above equations V_{rt} , V_{δ_1} and V_{δ_2} are the coefficients of variation (COVs) of the calculated resistance and the error terms δ_1 and δ_2 , respectively. $V_{\delta_1} = 0.071$ and $V_{\delta_2} = 0.018$ were obtained using the respective data sets of 660 and 4 points. To determine V_{rt} a Taylor series approximation was used (in accordance with Eurocode 0 guidance) and the first term in each basic variable κ_i was maintained. The variables κ_i included the thickness t , the web depth h , the flange width b , the lip length c , the elastic modulus E and the yield stress f_y . Consequently, V_{rt} was determined by:

$$\begin{aligned} V_{rt}^2 &= \frac{1}{r_m^2} \left(\sum_{i=1}^j \frac{\partial r}{\partial \kappa_i} \sigma_i \right)^2 \\ &= \frac{1}{r_m^2} \left[\left(\frac{\partial M_c}{\partial t} \sigma_t \right)^2 + \left(\frac{\partial M_c}{\partial h} \sigma_h \right)^2 + \left(\frac{\partial M_c}{\partial b} \sigma_b \right)^2 + \left(\frac{\partial M_c}{\partial c} \sigma_c \right)^2 + \left(\frac{\partial M_c}{\partial E} \sigma_E \right)^2 + \left(\frac{\partial M_c}{\partial f_y} \sigma_{f_y} \right)^2 \right] \end{aligned} \quad (23)$$

In Eq. (23) the σ_i are the standard deviations of the basic variables κ_i . Representative values were obtained from [48] and these are listed in Table 7. The partial derivatives in Eq. (23) were numerically calculated by replacing them by finite differences:

$$\frac{\partial M_c}{\partial \kappa_i} = \frac{\Delta M_c}{\Delta \kappa_i} \quad (24)$$

The parameters α_{rt} , α_{δ_1} and α_{δ_2} in Eq. (13) are weighting factors for Q_{rt} , Q_{δ_1} and Q_{δ_2} , respectively, obtained as:

$$\alpha_{rt} = \frac{Q_{rt}}{Q} \quad (25)$$

$$\alpha_{\delta_1} = \frac{Q_{\delta_1}}{Q} \quad (26)$$

$$\alpha_{\delta_2} = \frac{Q_{\delta_2}}{Q} \quad (27)$$

Based on Eq. (13) the partial safety factors γ were calculated for two distinct cases: (i) the case where the individual equations (Eqs. 8-10) were used, depending on the bolt group configuration, and (ii) the case where the general equation (Eq. 11) was applied to all data points. In both cases an average partial safety factor γ of 1.01 was obtained. This is very

close to the (lowest possible) γ value of 1.00, recommended by Eurocode 3 and adopted by most EU member states. It can thus be concluded that the proposed equations (Eqs. 8-10) are safe for use in conjunction with the Eurocode standards.

On the other hand, according to the North-American AISI [47] standard the resistance factor ϕ is calculated as:

$$\phi = C_{\phi} (M_m F_m P_{m1} P_{m2}) e^{-\beta_0 \sqrt{V_M^2 + V_F^2 + C_{p1} V_{p1}^2 + C_{p2} V_{p2}^2 + V_Q^2}} \quad (28)$$

In the above equation $C_{\phi}=1.52$ [44]. M_m (= 1.1) and F_m (= 1.0) are the mean values of the material and fabrication factors, and $V_M=0.1$ and $V_F=0.05$ are the corresponding COVs, respectively [47, 50]. The professional factor P_m in the original AISI equation was replaced by the product of P_{m1} and P_{m2} . P_{m1} is the mean ratio of the FE predicted capacity to the capacity calculated with the proposed design equation (M_{FE}/M_c), and P_{m2} is the mean ratio of the experimentally measured capacity to the corresponding FE prediction (M_{Test}/M_{FE}). V_{p1} and V_{p2} are the corresponding COVs (equivalent to $V_{\delta1}$ and $V_{\delta2}$ in the Eurocode procedure). V_Q is the COV of the loading and can be taken as 0.21 for CFS structures [47]. The C_p factors account for the samples sizes and are defined by:

$$C_p = \frac{n+1}{n} \frac{n-1}{n-3} \quad (29)$$

With respective sample sizes of 660 and 4, $C_{p1}=1.005$ and $C_{p2}=3.75$ were obtained using the above equation.

With the cross-sectional bending capacity M_u in Eq. (5) calculated according to the AISI effective width provisions, a resistance factor $\phi=0.94$ was obtained. This factor exceeds the value of 0.9 prescribed by the AISI design rules for CFS flexural members, demonstrating that the proposed design rules can safely be used within this context.

The AISI rules also allow the option of determining M_u using the Direct Strength Method [44] and when this option was used, a resistance factor $\phi=0.98$ was obtained. This value again exceeds the specified value of 0.9, indicating a safe design procedure.

5 Summary and conclusions

This paper presents a novel design methodology applicable to bolted connections in CFS flexural members where failure occurs due to localized buckling in the beam. Practical design equations were developed with the support of detailed GMNIA FE models, which were first validated against experiments on CFS apex connections in four-point bending. Comprehensive parametric studies were conducted covering an extensive range of the

governing parameters, namely the cross-sectional geometry (reflected in the eccentricity X , the web depth h and the thickness t), the bolt group length l_b and the bolt group configuration. The results indicated that the ultimate moment capacity of the CFS beam may be reduced by up to 40% for short bolt group lengths as a result of premature local buckling failure. However, as the bolt group length increases the capacity loss decreases exponentially. The argument is put forward that the modified stress distribution encountered adjacent to the connection and precipitating premature buckling is the result of a shear lag effect, rather than being caused by the workings of a bi-moment (as is the current governing opinion in literature). Finally, the results of a reliability analysis are presented, carried out within both the frameworks of the Eurocode and the AISI specifications, to demonstrate that the proposed equations are safe for use in practical design.

Acknowledgement

This research was supported by the Engineering and Physical Sciences Research Council (EPSRC) grants EP/L019116/1 and EP/M011976/1. The first author was also supported by EPSRC Doctoral Scholarship grant 1625179.

References

- [1] L.W. Williams, 1 - Introduction to recent trends in cold-formed steel construction A2 - Yu, Cheng, in: *Recent Trends in Cold-Formed Steel Construction*, Woodhead Publishing, 2016, pp. 1-35.
- [2] S.M. Mojtabaei, M.Z. Kabir, I. Hajirasouliha, M. Kargar, Analytical and experimental study on the seismic performance of cold-formed steel frames, *Journal of Constructional Steel Research*, 143 (2018) 18-31.
- [3] J.B.P. Lim, D.A. Nethercot, Finite element idealization of a cold-formed steel portal frame, *Journal of Structural Engineering*, 130 (2004) 78-94.
- [4] A.B. Sabbagh, R. Mirghaderi, M. Petkovski, K. Pilakoutas, An integrated thin-walled steel skeleton structure (two full scale tests), *Journal of Constructional Steel Research*, 66 (2010) 470-479.
- [5] D. Dubina, A. Stratan, Z. Nagy, Full-scale tests on cold-formed steel pitched-roof portal frames with bolted joints, *Advanced Steel Construction*, 5 (2009) 175-194.
- [6] P. Kirk, Design of a cold-formed section portal frame building system, *Proc. 8th International Speciality Conference on Cold-formed Steel Structures*, St. Louis, MO, University of Missouri-Rolla; p.295, (1986).
- [7] K.F. Chung, L. Lau, Experimental investigation on bolted moment connections among cold formed steel members, *Engineering Structures*, 21 (1999) 898-911.
- [8] J. Lim, Joint effects in cold-formed steel portal frames. University of Nottingham, PhD thesis, (2001).
- [9] J.B.P. Lim, D.A. Nethercot, Ultimate strength of bolted moment-connections between cold-formed steel members, *Thin Wall Structures*, 41 (2003) 1019-1039.

- [10] J.B.P. Lim, G.J. Hancock, G.C. Clifton, C.H. Pham, R. Das, DSM for ultimate strength of bolted moment-connections between cold-formed steel channel members, *Journal of Constructional Steel Research*, 117 (2016) 196-203.
- [11] A.H. Baigent, G.J. Hancock, Structural analysis of assemblages of thin-walled members, *Engineering Structures*, 4 (1982) 207-216.
- [12] M.F. Wong, K.F. Chung, Structural behaviour of bolted moment connections in cold-formed steel beam-column sub-frames, *Journal of Constructional Steel Research*, 58 (2002) 253-274.
- [13] F. Öztürk, S. Pul, Experimental and numerical study on a full scale apex connection of cold-formed steel portal frames, *Thin-Walled Structures*, 94 (2015) 79-88.
- [14] Ž. Bučmys, A. Daniūnas, J.-P. Jaspart, J.-F. Démonceau, A component method for cold-formed steel beam-to-column bolted gusset plate joints, *Thin-Walled Structures*, 123 (2018) 520-527.
- [15] A. Bagheri Sabbagh, M. Petkovski, K. Pilakoutas, R. Mirghaderi, Experimental work on cold-formed steel elements for earthquake resilient moment frame buildings, *Engineering Structures*, 42 (2012) 371-386.
- [16] Rinchen, K.J.R. Rasmussen, Behaviour and modelling of connections in cold-formed steel single C-section portal frames, *Thin-Walled Structures*, 143 (2019) 106233.
- [17] R. Rinchen, K.J.R. Rasmussen, Experiments on Long-Span Cold-Formed Steel Single C-Section Portal Frames, *Journal of Structural Engineering*, 146 (2020) 04019187.
- [18] Rinchen, K.J.R. Rasmussen, Numerical modelling of cold-formed steel single C-section portal frames, *Journal of Constructional Steel Research*, 158 (2019) 143-155.
- [19] Rinchen, K.J.R. Rasmussen, H. Zhang, Design of cold-formed steel single C-section portal frames, *Journal of Constructional Steel Research*, 162 (2019) 105722.
- [20] H.B. Blum, K.J.R. Rasmussen, Experimental investigation of long-span cold-formed steel double channel portal frames, *Journal of Constructional Steel Research*, 155 (2019) 316-330.
- [21] H.B. Blum, K.J.R. Rasmussen, Experimental and numerical study of connection effects in long-span cold-formed steel double channel portal frames, *Journal of Constructional Steel Research*, 155 (2019) 480-491.
- [22] X. Zhang, K.J.R. Rasmussen, H. Zhang, Experimental investigation of locally and distortionally buckled portal frames, *Journal of Constructional Steel Research*, 122 (2016) 571-583.
- [23] X. Zhang, K.J.R. Rasmussen, H. Zhang, Structural modeling of cold-formed steel portal frames, *Structures*, 4 (2015) 58-68.
- [24] B. Tshuma, M. Dundu, Internal eaves connections of double-bay cold-formed steel portal frames, *Thin-Walled Structures*, 119 (2017) 760-769.
- [25] P. Pouladi, J. Ronaldson, G.C. Clifton, J.M. Ingham, A.M. Wrzesien, J.B.P. Lim, Finite-element assisted design of eaves joint of cold-formed steel portal frames having single channel-sections, *Structures*, 20 (2019) 452-464.
- [26] J.B.P. Lim, D.A. Nethercot, Stiffness prediction for bolted moment-connections between cold-formed steel members, *Journal of Constructional Steel Research*, 60 (2004) 85-107.
- [27] A. Bagheri Sabbagh, M. Petkovski, K. Pilakoutas, R. Mirghaderi, Cyclic behaviour of bolted cold-formed steel moment connections: FE modelling including slip, *Journal of Constructional Steel Research*, 80 (2013) 100-108.
- [28] I. Elkersh, Experimental investigation of bolted cold formed steel frame apex connections under pure moment, *Ain Shams Engineering Journal*, 1 (2010) 11-20.
- [29] M.H. Serror, E.M. Hassan, S.A. Mourad, Experimental study on the rotation capacity of cold-formed steel beams, *J Constr Steel Res*, 121 (2016) 216-228.
- [30] J. Ye, S.M. Mojtabaei, I. Hajirasouliha, K. Pilakoutas, Efficient design of cold-formed steel bolted-moment connections for earthquake resistant frames, *Thin-Walled Structures*, (2019).

- [31] J. Ye, S.M. Mojtabaei, I. Hajirasouliha, Seismic performance of cold-formed steel bolted moment connections with bolting friction-slip mechanism, *Journal of Constructional Steel Research*, 156 (2019) 122-136.
- [32] A. Bagheri Sabbagh, M. Petkovski, K. Pilakoutas, R. Mirghaderi, Development of cold-formed steel elements for earthquake resistant moment frame buildings, *Thin-Walled Structures*, 53 (2012) 99-108.
- [33] M.R. Haidarali, D.A. Nethercot, Finite element modelling of cold-formed steel beams under local buckling or combined local/distortional buckling, *Thin Wall Structures*, 49 (2011) 1554-1562.
- [34] B.P. Gilbert, K.J.R. Rasmussen, Bolted moment connections in drive-in and drive-through steel storage racks, *Journal of Constructional Steel Research*, 66 (2010) 755-766.
- [35] R. Gutierrez, A. Loureiro, J.M. Reinoso, M. Lopez, Numerical study of purlin joints with sleeve connections, *Thin-Walled Structures*, 94 (2015) 214-224.
- [36] Q. Liu, J. Yang, F.L. Wang, Numerical simulation of sleeve connections for cold formed steel sigma sections, *Engineering Structures*, 100 (2015) 686-695.
- [37] Abaqus/CAE User's Manual, version 6.7, USA., (2007).
- [38] J.W. Fisher, On the Behavior of Fasteners and Plates with Holes, in, Fritz Engineering Laboratory, Department of Civil Engineering, Lehigh University, 1964.
- [39] C.M. Uang, A. Sato, J.K. Hong, K. Wood, Cyclic Testing and Modeling of Cold-Formed Steel Special Bolted Moment Frame Connections, *J Struct Eng-Asce*, 136 (2010) 953-960.
- [40] B.W. Schafer, T. Peköz, Computational modeling of cold-formed steel: characterizing geometric imperfections and residual stresses, *Journal of Constructional Steel Research*, 47 (1998) 193-210.
- [41] A.C. Walker, Design and analysis of cold-formed sections, Halsted Press, 1975.
- [42] Z. Li, B.W. Schafer, Buckling analysis of cold-formed steel members with general boundary conditions using CUFSM conventional and constrained finite strip methods, (2010).
- [43] Y. Shifferaw, B.W. Schafer, Inelastic Bending Capacity of Cold-Formed Steel Members, *Journal of Structural Engineering*, 138 (2012) 468-480.
- [44] AISI S100-12, North American specification for the design of cold-formed steel structural members, American Iron and Steel Institute (AISI), Washington, DC, USA, (2012).
- [45] Mathworks, Matlab R2015b, Mathworks Inc., (2015).
- [46] CEN, Eurocode 0: "Basis of structural design." , European Committee for Standardization, Brussels, (2002).
- [47] L.E. Hsiao, W.W. Yu, T.V. Galambos, AISI LRFD method for cold-formed steel structural members, 9th Int. Specialty Conf. on Cold-Formed Steel Structures, (1988).
- [48] B. Young, G. Hancock, Design of Cold-Formed Channels Subjected to Web Crippling, *J. Struct. Eng.*, 127(10) (2001) 1137-1144.
- [49] F.J. Meza, J. Becque, I. Hajirasouliha, Experimental study of cold-formed steel built-up columns, *Thin-Walled Structures* (in press), (2019).
- [50] C.H Pham, G.J. Hancock, Direct strength design of cold-formed C-sections for shear and combined actions, 138(6) (2012) 759–768.

List of Figures

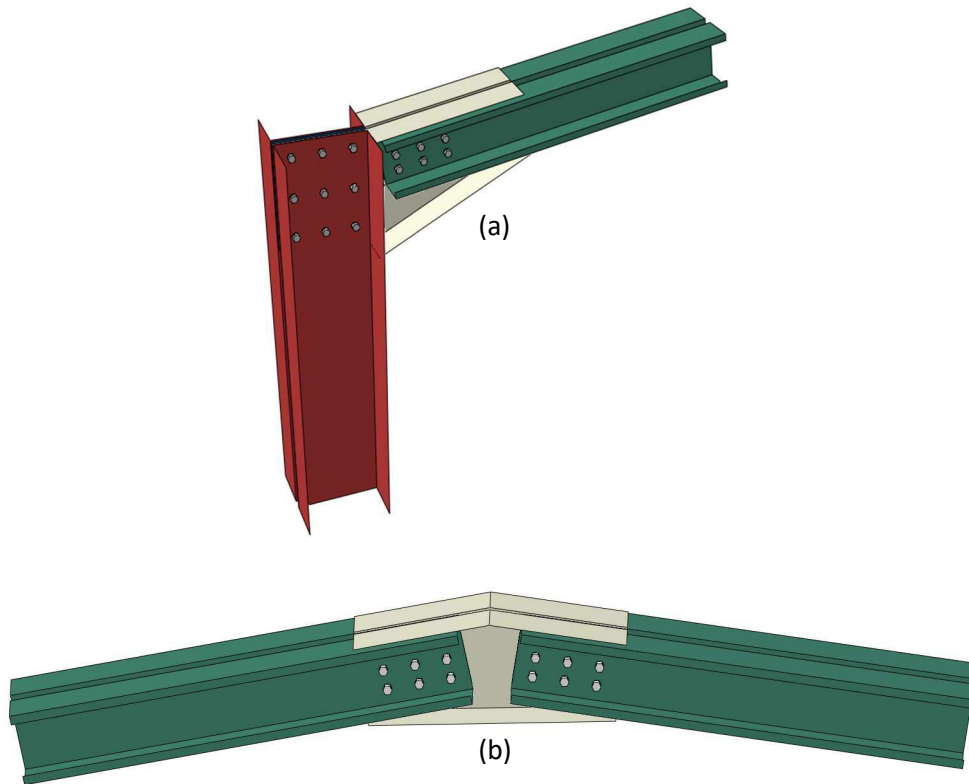


Fig. 1: Typical CFS moment resisting bolted connections: (a) eaves connection, and (b) apex connection

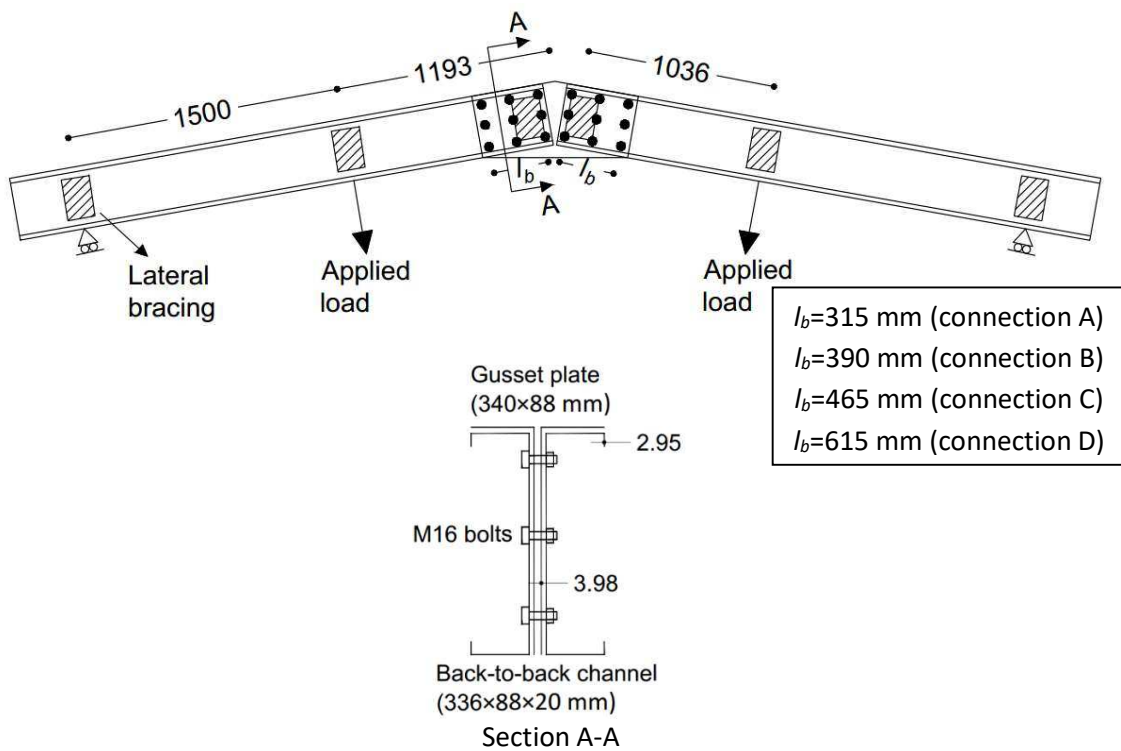


Fig. 2: Apex connections tested by Lim and Nethercot [9]

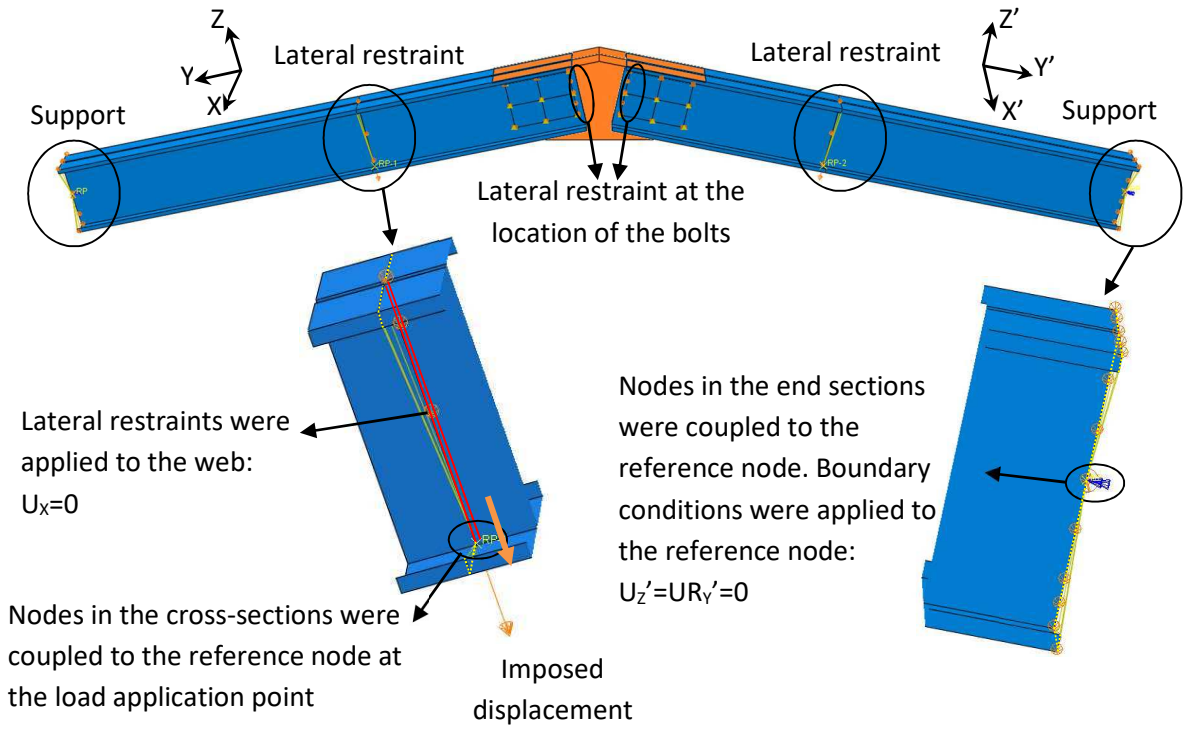


Fig. 3: FE model of apex connection showing loading and boundary conditions

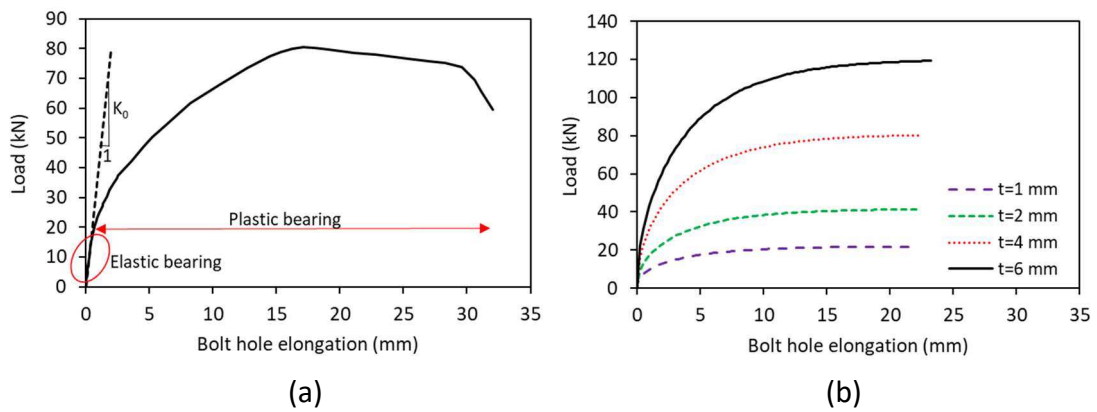


Fig. 4: Bearing behaviour of bolt against steel plate adopted from: (a) tests conducted by Lim and Nethercot [26], and (b) Eq. 1, proposed by Fisher [38]

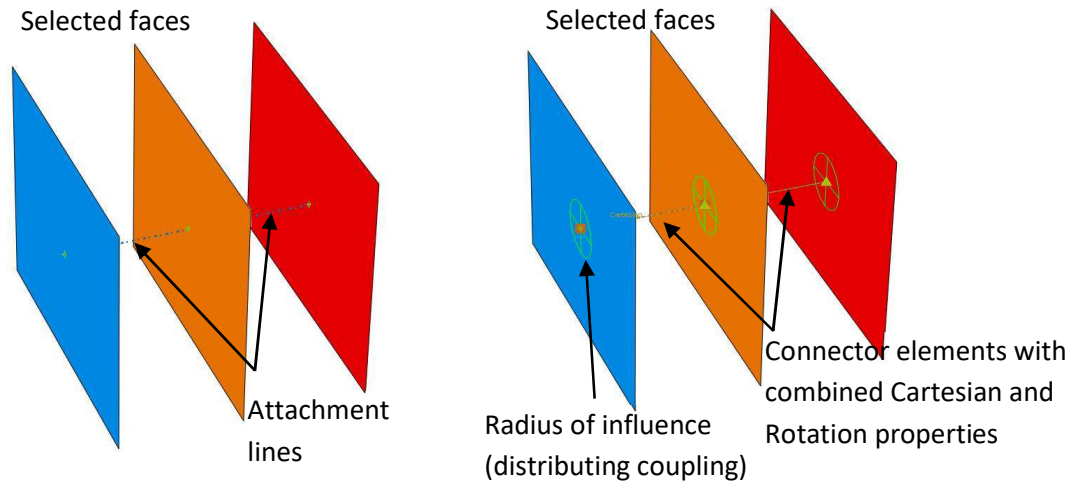


Fig. 5: Modelling a single bolt with discrete fastener elements

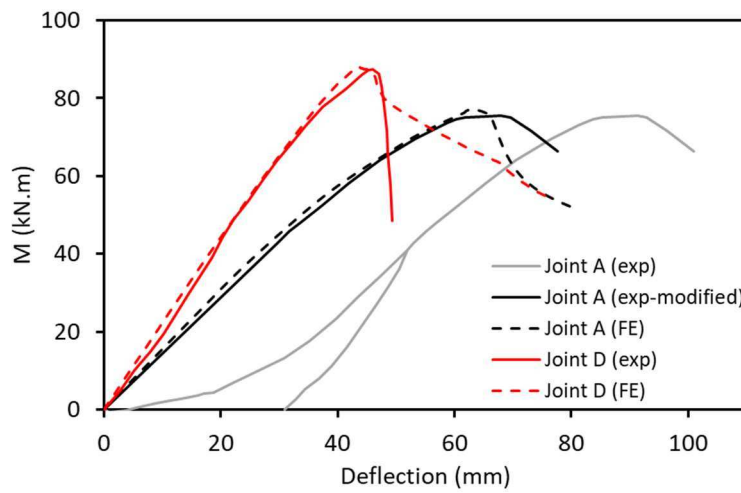


Fig. 6: Comparison of moment-deflection curves of apex connections obtained from tests and FE simulations

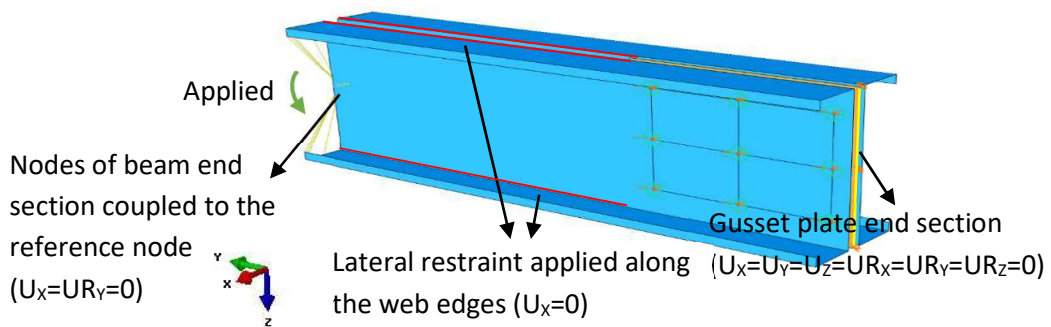


Fig. 7: FE model of simplified moment-resisting bolted connection including loading and boundary conditions

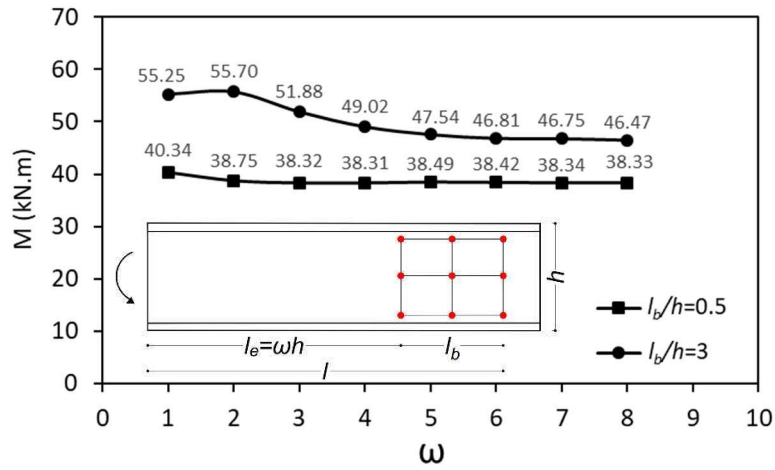


Fig. 8: Sensitivity study of the cantilever length for two different bolt group sizes ($l_b/h = 0.5$ and $l_b/h = 3$)

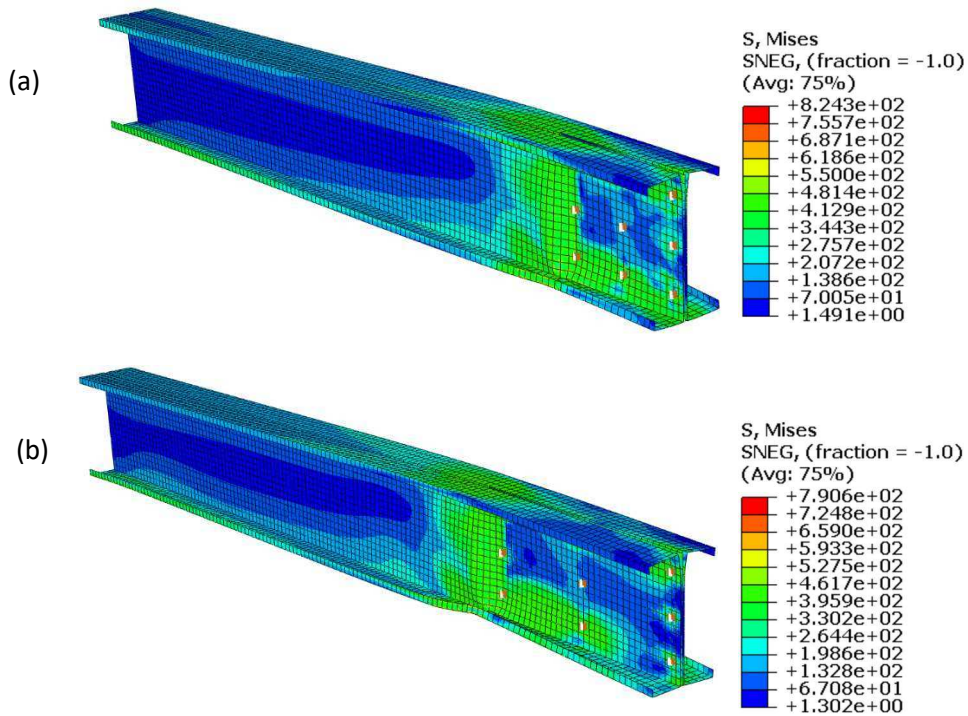


Fig. 9: Connection failure modes obtained from simplified FE models: (a) connection A, (b) connection D

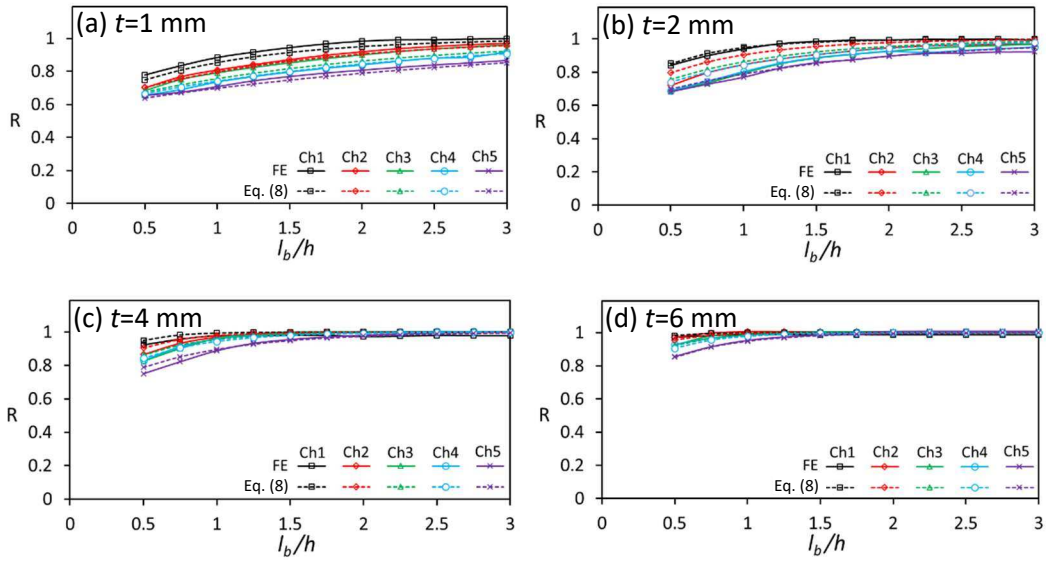


Fig. 10: Flexural capacity of CFS moment resisting bolted connections with rectangular 2x2 bolt group configuration and various bolt group lengths and cross-sectional eccentricities

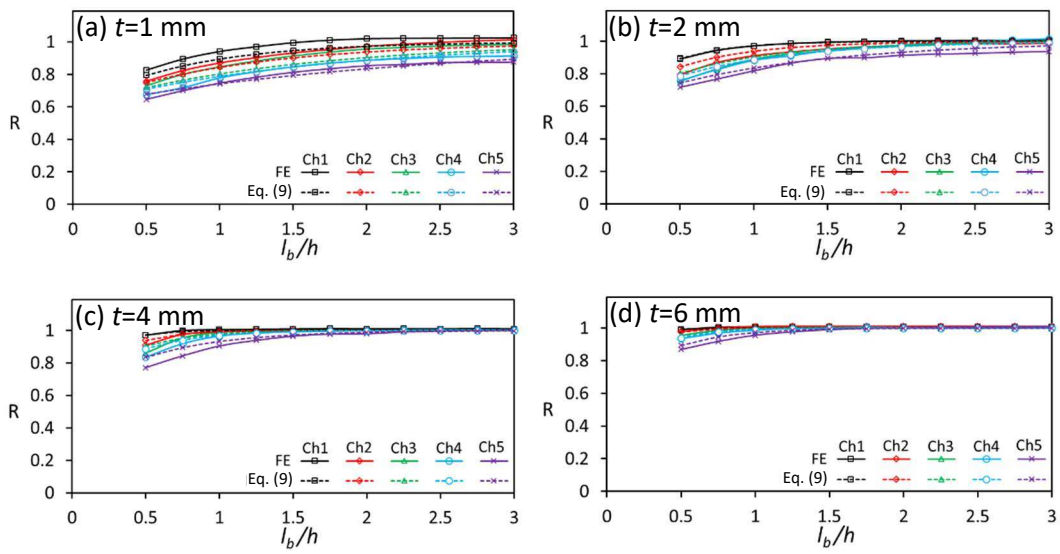


Fig. 11: Flexural capacity of CFS moment resisting bolted connections with rectangular 3x3 bolt group configuration and various bolt group lengths and cross-sectional eccentricities

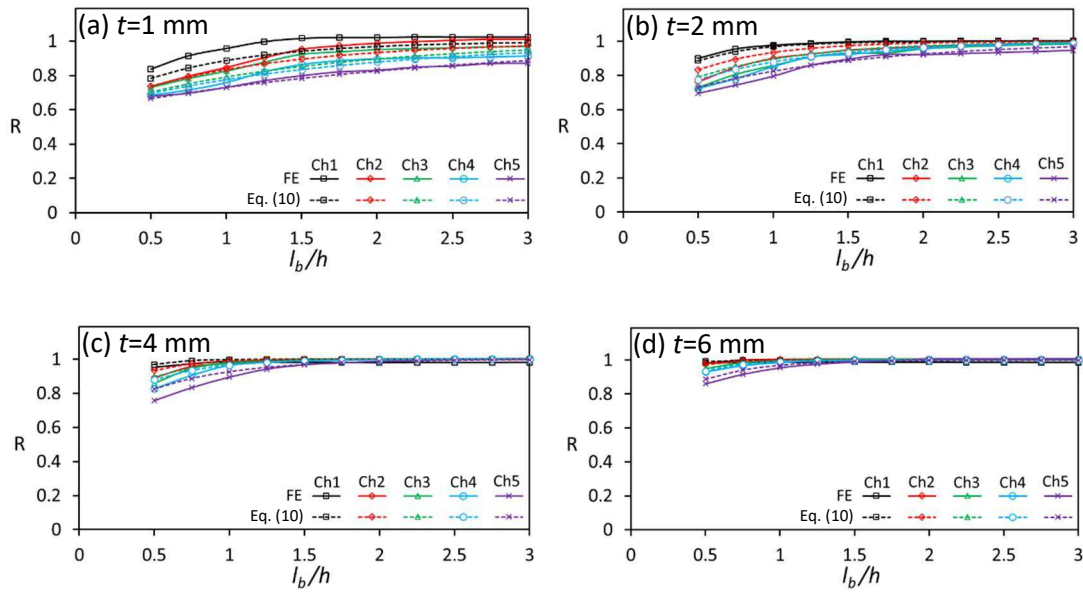


Fig. 12: Flexural capacity of CFS moment resisting bolted connections with rectangular 4x4 bolt group configuration and various bolt group lengths and cross-sectional eccentricities

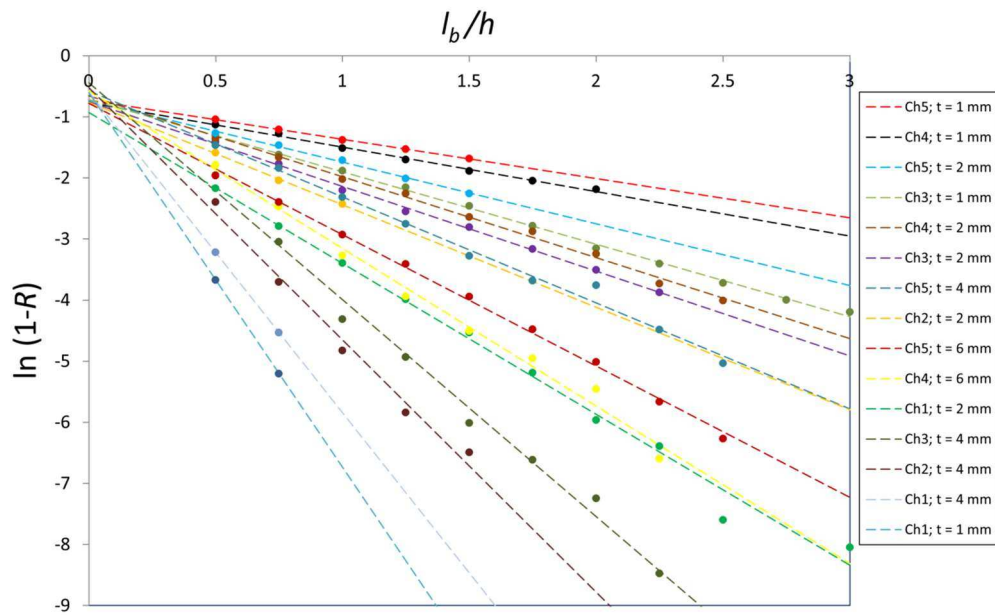


Fig. 13: FE data in semi-logarithmic format for a 3x3 bolt group. The various colours indicate results for various channel geometries and thicknesses.

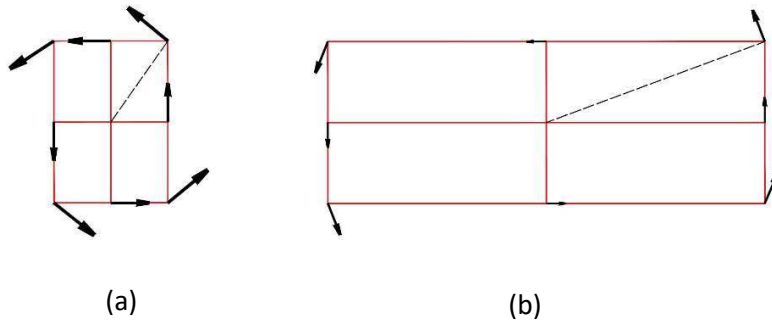


Fig. 14. Schematic distribution of bolt forces in: (a) a short bolt group, and (b) a long bolt group

List of Tables

Table 1: Mesh sensitivity analysis of connection D

Mesh size (mm x mm)	Predicted capacity M_{max}^{FE} (kN.m)
10×10	87.69
15×15	87.80
20×20	88.02
30×30	91.91
40×40	93.06

Table 2: Comparison of the flexural capacities of the connections obtained from tests and FE simulations

connection	l_b (mm)	l_b/h	M_{max}^{exp} (kN.m)	M_{max}^{FE} (kN.m)	$M_{max}^{FE}/M_{max}^{exp}$	$M_{max}^{s,FE}$	$M_{max}^{s,FE}/M_{max}^{exp}$
A	315	0.94	75	76.01	1.01	75.92	1.01
B	390	1.16	77.5	80.72	1.04	80.39	1.04
C	465	1.38	82.5	82.5	1.00	81.55	0.99
D	615	1.83	87.5	88.02	1.01	85.36	0.98
Average					1.02		1.00
St. dev					0.018		0.027

Table 3: Selected variables for parametric studies

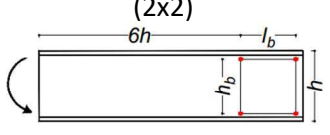
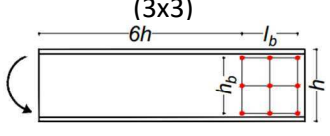
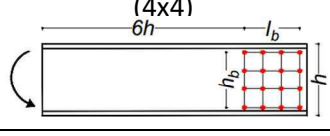
Variables			
Beam channel section	Thickness	Bolt configuration	Bolt group size
Ch1	$t = 1, 2, 4, 6$ mm	(2x2) 	$\frac{h_b}{h} = 0.8$ $\frac{l_b}{h} = [0.5, 0.75, 1, 1.25, 1.5, 1.75, 2, 2.25, 2.5, 2.75, 3]$
Ch2		(3x3) 	
Ch3		(4x4) 	
Ch4			
Ch5			

Table 4: Dimensions and cross-sectional capacity of various CFS back-to-back channel sections

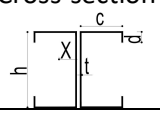
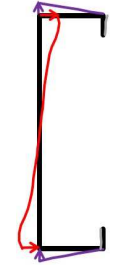
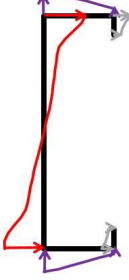

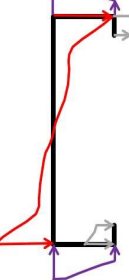
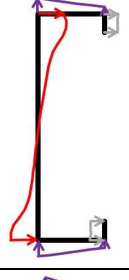
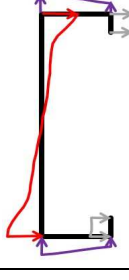
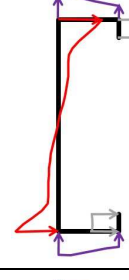
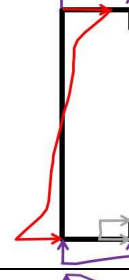
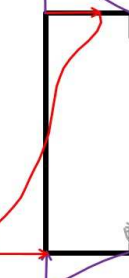

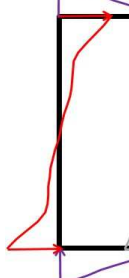
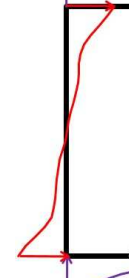

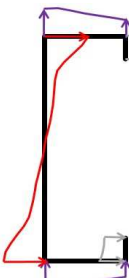
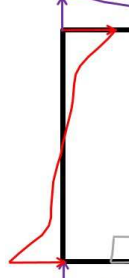


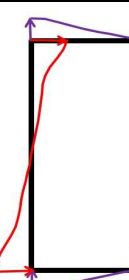
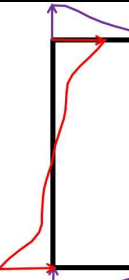
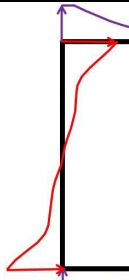
Cross-section 	X (mm)	Dimensions			t (mm)	λ_s	M_u (kN.m)
		h (mm)	c (mm)	d (mm)			
Ch1	11.11	300	50	25	1	2.047	15.26
					2	1.033	44.05
					4	0.572	107.15
					6	0.436	168.00
Ch2	15.71	250	60	25	1	1.724	12.97
					2	0.863	39.30
					4	0.524	88.59
					6	0.405	135.41
Ch3	20.83	250	75	25	1	1.752	13.08
					2	0.877	41.81
					4	0.575	96.13
					6	0.446	147.72
Ch4	23.44	200	75	25	1	1.521	10.63
					2	0.798	30.69
					4	0.536	70.77
					6	0.418	108.60
Ch5	33.33	200	100	25	1	1.844	10.78
					2	0.970	32.89
					4	0.658	80.86
					6	0.514	123.96

Table 5: Proposed reduction factors for different bolt group configurations

No. Eq.	Bolt group configuration	Reduction factor (R)	R_{pred}/R_{FE}	
			Average	COV
8	2x2	$R = 1 - 0.43e^{(-11.9(\frac{t}{X})(\frac{b}{h}))}$	1.01	0.08
9	3x3	$R = 1 - 0.40e^{(-14.9(\frac{t}{X})(\frac{b}{h}))}$	0.99	0.09
10	4x4	$R = 1 - 0.42e^{(-14.5(\frac{t}{X})(\frac{b}{h}))}$	1.00	0.08

Table 6: FE elastic stress profile in the beam for different bolt group lengths, thicknesses and eccentricities

Channel type	Bolt group length	Thickness			
		1 mm	2 mm	4 mm	6 mm
Ch1	$l_b/h = 0.5$				
	$l_b/h = 3$				
Ch2	$l_b/h = 0.5$				
	$l_b/h = 3$				
Ch3	$l_b/h = 0.5$				

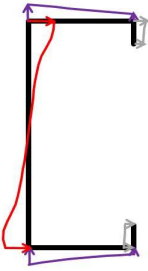
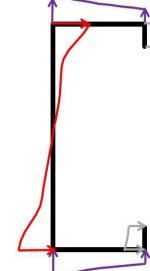
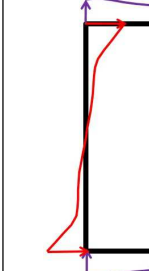
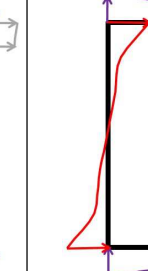
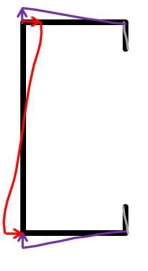
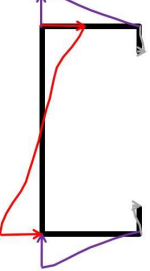
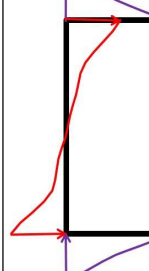
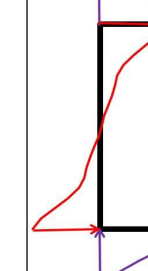
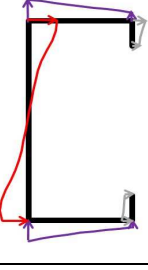
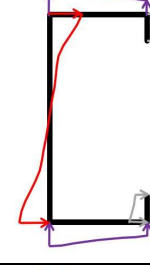
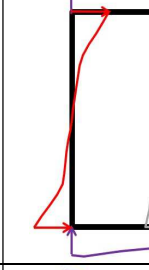
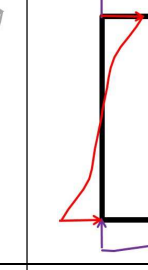

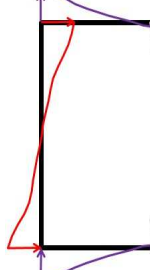
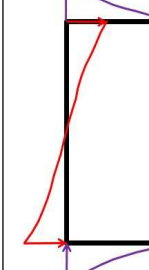
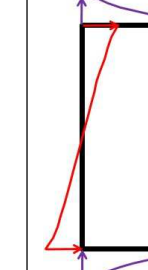
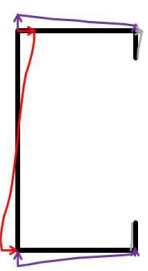
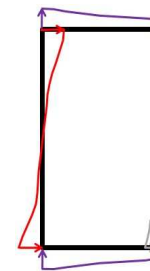
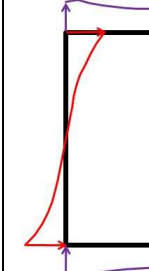
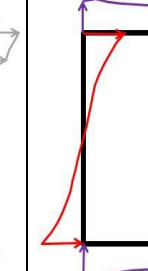
	$l_b/h = 3$				
Ch4	$l_b/h = 0.5$				
	$l_b/h = 3$				
Ch5	$l_b/h = 0.5$				
	$l_b/h = 3$				

Table 7: Statistical distributions used in reliability analysis

Variable	Distribution	Nominal	Mean	σ	COV	References
E	Normal	E	E	$0.03E$	0.03	Young et al. [48]
f_y	Lognormal	f_y	$1.1f_y$	$0.0693f_y$	0.063	Young et al. [48]
t	Normal	t	t	$0.005t$	0.005	Meza et al. [49]
h	Normal	h	h	$0.005h$	0.005	Meza et al. [49]
b	Normal	b	b	$0.002b$	0.002	Meza et al. [49]
c	Normal	c	c	$0.02c$	0.02	Meza et al. [49]